IOP Publishing Journal of Physics: Condensed Matter
J. Phys.: Condens. Matter **32** (2020) 205801 (7pp) https://doi.org/10.1088/1361-648X/ab6e93

Investigation of 2π isolated skyrmion pinning using exchange bias

Haiyan Xia[1], Jinshuai Wang[1], Chengkun Song[1], Chendong Jin[1], Yunxu Ma[1], Chunlei Zhang[1], Jianing Wang[1], Yurui Wei[1], Jianbo Wang[1,2] and Qingfang Liu[1,3]

[1] Key Laboratory for Magnetism and Magnetic Materials of the Ministry of Education, Lanzhou University, Lanzhou 730000, People's Republic of China
[2] Key Laboratory of Special Function Materials and Structure Design, Ministry of Education, Lanzhou University, Lanzhou 730000, People's Republic of China

E-mail: liuqf@lzu.edu.cn

Received 15 November 2019, revised 4 January 2020
Accepted for publication 22 January 2020
Published 20 February 2020

Abstract

The 2π isolated chiral skyrmion is a magnetic configuration. Since the total topological charge is zero, the 2π isolated skyrmion driven by a spin-polarized current propagates strictly along the racetrack. The manipulation of 2π-skyrmion, e.g., pinning/depinning at a specific position of the racetrack, is significant. Here, we investigated the 2π-skyrmion pinning in a racetrack using exchange bias. A series of transversal AFM wires were set above the ferromagnetic (FM) racetrack. Spin waves were employed to induce 2π-skyrmion motion to study the dynamics of the 2π-skyrmion pinning. The AFM wires induce exchange bias at the AFM/FM crossing points, which can act as pinning sites. The working window for a 2π-skyrmion in a racetrack was investigated as a function of the exchange bias field, the frequency and amplitude of the oscillating magnetic field for exciting spin waves. The interaction mechanism between the 2π-skyrmion and the exchange bias was also studied. This work may provide guidance for the design of next-generation spintronics.

Keywords: 2π-skyrmion, antiferromagentic materials, pinning/depinning, racetrack memory

(Some figures may appear in colour only in the online journal)

1. Introduction

Magnetic skyrmions are stable topologically spin configurations, which have become the focus of intense research activities over the last years due to their promising applications in spintronic devices [1–3]. Common isolated skyrmions (π skyrmion) and multi-π skyrmion belong to a set of solutions of the basic equation for skyrmions [4]. Multi-π skyrmions have been introduced and investigated in [4]. Recent experimental advances in the observation of 2π-skyrmion states in ferromagnetic (FM) films have renewed the interest to this special spin configuration and triggered intensive theoretical studies of static and dynamic 2π-skyrmions [5–9]. Particularly, the 2π skyrmions have been observed in FM materials [5–9], such as $Tb_{22}Fe_{69}Co_9$ thin films [7], Cr:Sb_2Te_3/FeNi FM-magnetic insulator heterostructure [5], FeGe nanodisks [8], Pd_2/Fe/Ir(1 1 1) island [6] and asymmetric Ir/Co/Pt multilayers [9].

Since the total topological charge $Q = 0$, the 2π-skyrmion driven by a spin-polarized current can propagates strictly along the racetrack without obvious deformation [10, 11]. This intriguing characteristic makes 2π-skyrmion as a promising information carrier for next-generation spintronic devices, especially for racetrack memory [10,11]. In addition, the 2π skyrmion is stable even in the absence of external magnetic field, which is significant for the design of skyrmion-based spintronics [12]. Up to now, the fundamental behaviors, including nucleation/annihilation, motion and detection of 2π-skyrmions have been intensively investigated, which are significantly different from those of skyrmions [5, 10–15].

[3] Author to whom any correspondence should be addressed.

The manipulation of skyrmions, e.g., pinning/depinning at a specific position of the racetracks, is significant for racetrack memory [16–20]. When skyrmions are generated, the skyrmion positions are deterministic in most cases. If one relies on natural pinning sites of the materials, the skyrmions are in random positions [16, 20, 21]. By using artificial pinning sites, the positions of skyrmions can be controlled more precisely [16, 17]. Furthermore, the artificial pinning sites can enhance the stability against thermal fluctuation and stray field [17, 22]. Until now, the pinning/depingning of a 2π-skyrmion remains an open question [14]. In this work, we report a simple pinning scheme for 2π-skyrmions using exchange bias. A series of transversal AFM wires were set above the FM racetrack. The AFM wires induce exchange bias at the AFM/FM crossing points, which can act as pinning sites. The strength of 2π-skyrmions pins can be modulated by the exchange bias field. Such a system has been experimentally reported for domain wall pinning and has the advantage of ease of fabrication [22].

2. Model and simulations

Micromagnetic simulations were performed by using the object-oriented micromagnetic framework (OOMMF), including the extension Dzyaloshinskii–Moriya interaction (DMI) module [23, 24]. The modified Landau–Lifshitz–Gilbert equation is written as:

$$\frac{\mathrm{d}\mathbf{m}}{\mathrm{d}t} = -|\gamma|\,\mathbf{m}\times\mathbf{H}_{\mathrm{eff}} + \alpha\left(m\times\frac{\mathrm{d}\mathbf{m}}{\mathrm{d}t}\right) \quad (1)$$

where $\mathbf{m} = M/M_{\mathrm{s}}$ is the normalized magnetization vector with M_{s} the saturation magnetization; γ is the gyromagnetic ratio which equals to 2.211×10^{5} m $(\mathrm{A}\cdot\mathrm{s})^{-1}$); H_{eff} is the effective field; α is damping constant. The effective field H_{eff} is comprised of Heisenberg exchange, magnetic anisotropy, demagnetization, DMI and external magnetic field. The DMI energy density is given as [24]:

$$\varepsilon_{\mathrm{DM}} = \mathcal{D}\left(m_z\frac{\partial m_x}{\partial x} - m_x\frac{\partial m_z}{\partial x} + m_z\frac{\partial m_y}{\partial y} - m_y\frac{\partial m_z}{\partial y}\right) \quad (2)$$

where m_x, m_y and m_z are the components of normalized magnetization and $\mathcal{D}$ is the continuous effective DMI parameter.

The FM racetrack is in dimension of 2000 nm × 100 nm × 1 nm (length × width × thickness). The mesh cell is 2 nm × 2 nm × 1 nm. The default magnetic material parameters are adopted as follows [9, 13, 15]: exchange constant $A = 1.5\times10^{-11}$ J m^{-1}; saturation magnetization $M_{\mathrm{s}} = 580\times10^{3}$ A m^{-1}; perpendicular anisotropy constant $K = 0.8\times10^{6}$ J m^{-3}. The DMI parameter is 3.5 mJ m^{-2} and the damping constant is 0.01.

The AFM wires are in dimension of 100 nm × 100 nm × 2 nm (length × width × thickness). The first AFM wire is located at $x = 1050$ nm and the spacing between AFM wires is 100 nm. Experiments demonstrate that after magnetic-field cooling, the CoPt/IrMn multilayer exhibits an out-of-plane magnetization and a clear perpendicular exchange bias (3.39 mT–8.12 mT) [25]. The perpendicular exchange bias can be expressed as [26, 27]: $H_{\mathrm{E}} = JS_{\mathrm{AFM}}S_{\mathrm{FM}}/\left(\mu_0\alpha_{\mathrm{AFM}}^2 M_{\mathrm{FM}}t_{\mathrm{FM}}\right)$, where J is the interface exchange energy; α_{AFM}^2 is the AFM unit-cell size; M_{FM} is the magnetization of the FM; t_{FM} is the thickness of the FM; S_{AFM} and S_{FM} are the net magnetic moments along the film normal in the AFM and FM interfacial layers. According to the above references, [25], the perpendicular exchange bias H_{E} was set from −8mT to 8 mT in the simulations.

A stable 2π-skyrmion is generated and relaxed at the position of (1000 nm, 50 nm) [13]. Then, spin waves were employed to induce 2π-skyrmion motion to study the dynamics of the 2π-skyrmion pinning. Spin waves can propagate in metals and insulators, especially in insulators with low damping [13, 15]. To generate spin waves, an oscillating magnetic field $B_{\mathrm{m}}\sin(2\pi ft)$ along the y-direction has been locally applied at the end of the racetrack (80 nm $< x <$ 160 nm). The excitation field amplitude B_{m} increases from 100 mT to 1000 mT and the excitation frequency f arranges from 40 GHz to 180 GHz [13, 15].

3. Results and discussions

Since at low fields 2π-skyrmions are destroyed via a burst instability connected to a breathing mode [28], we initially investigate the stability of 2π-skyrmions under the exchange bias. Figure 1(c) shows the magnetization profile M_z (x), diameter and domain wall (DW) width of a 2π-skyrmion as a function of the exchange bias field H_{E}. The characteristic parameters diameter (D_{sk1} and D_{sk2}), and DW width (Δ_1 and Δ_2) are defined in figure 1(b). As can be seen from figure 1(c), the exchange bias field within a certain range can adjust the size and shape of the 2π-skyrmion slightly. When the H_{E} is along the $+z$-direction, namely, $H_{\mathrm{E}} > 0$ mT, the size of the 2π-skyrmion shrinks. When the H_{E} is along the $-z$-direction, namely, $H_{\mathrm{E}} < 0$ mT, the 2π-skyrmion size expands. The DW widths (Δ_1 and Δ_2) are almost unchanged.

To investigate the interaction mechanism between the 2π skyrmion and the exchange bias, we study the energy profile. Figure 2(a) demonstrates the changes of the total energy ΔE as a function of 2π-skyrmion positions, with four AFM wires above the FM racetrack. Here, the ΔE is defined as $\Delta E = E_{\mathrm{i}} - E_0$, where E_{i} represents the total energy of the FM racetrack that hosts the 2π-skyrmion at any position x, and E_0 is the reference energy, in which the 2π-skyrmion is located at the maximum possible distance from the AFM wires. As shown in figure 2, the ΔE is periodic when four AFM wires were set above the FM racetrack. In the case of $H_{\mathrm{E}} > 0$ mT, energy barriers are generated at the AFM/FM crossing area, which lead to off-centered pinning in the racetrack. The height of energy barriers increases with the H_{E} increasing. In the condition of $H_{\mathrm{E}} < 0$ mT, energy wells are created at the AFM/FM crossing area, which can capture the 2π skyrmion in a well centered position in the AFM/FM crossing area. The depth of energy wells increases with the H_{E} increasing. Hence, the AFM/FM crossing area can serve as pinning sites for 2π skyrmions from the energy point of view.

To qualitative analyze how the exchange bias field produces the energy barriers or energy wells, the energy changes of the

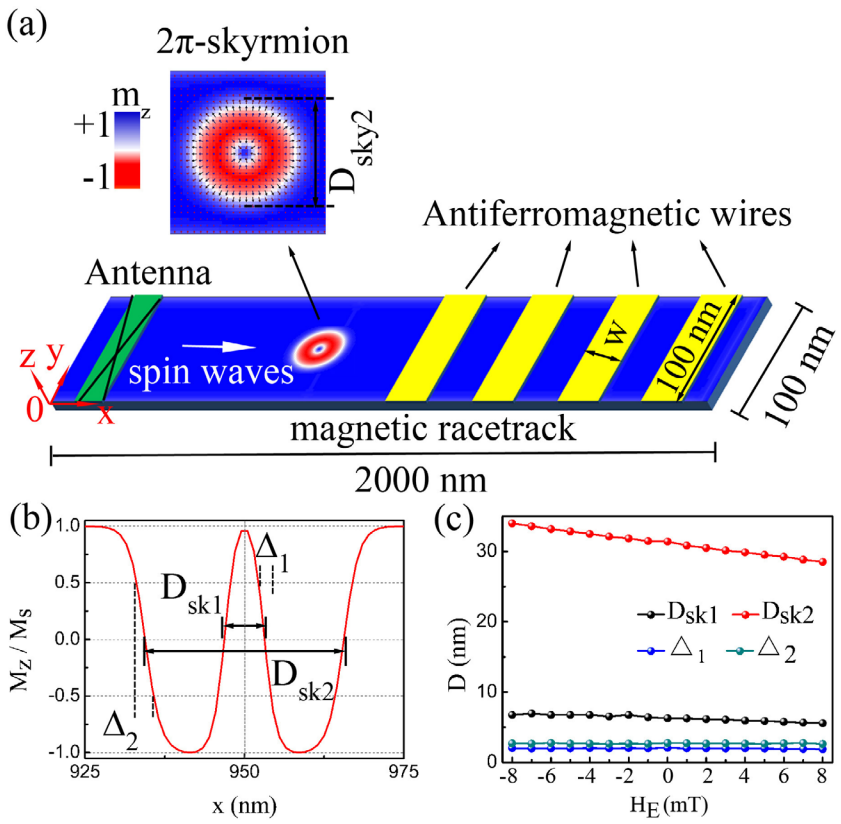

Figure 1. (a) The schematic diagram for micromagnetic simulations and the 2π-skyrmion configuration. The outer diameter of the 2π-skyrmion D_{sky2} and the width of the AFM wires w are defined here. (b) Magnetization profile M_z (x) along the diameter of a 2π-skyrmion and definition of the characteristic parameters diameter (D_{sk1} and D_{sk2}) and DW width (Δ_1 and Δ_2). (c) Diameter and DW width as a function of the exchange bias field.

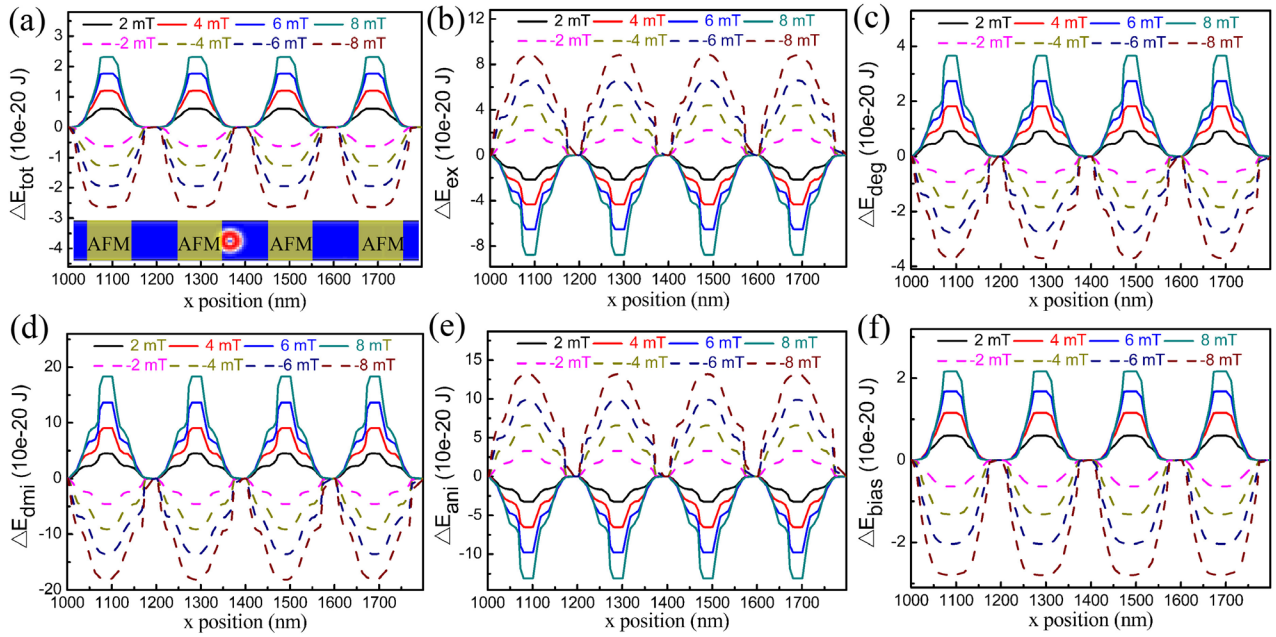

Figure 2. The changes of (a) the total energy, (b) the exchange energy, (c) the demagneting energy, (d) the DMI energy, (e) the anisotropy energy and (f) the bias field energy of the system as a function of the 2π-skyrmion with four AFM wires above the FM racetrack. The exchange bias field H_E ranges from -8 mT to 8 mT.

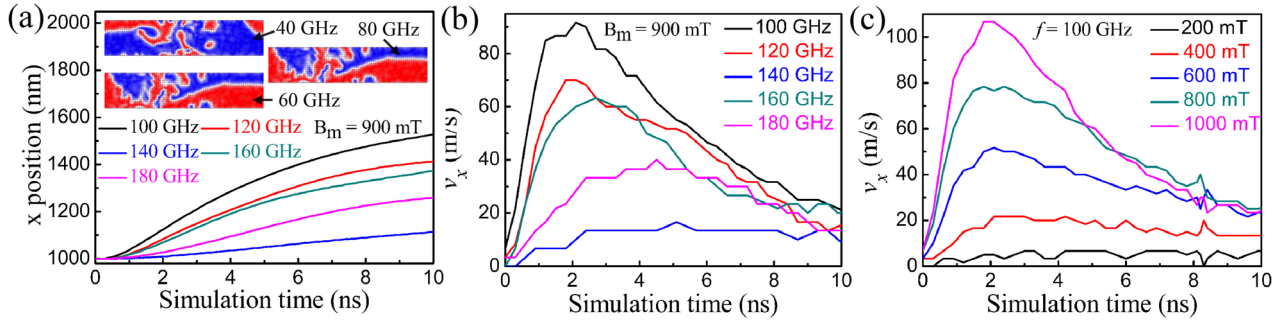

Figure 3. The 2π-skyrmion motion driven by spin waves. (a) The 2π-skyrmion position as a function of simulation time, where the insets show the top-view snapshots at selected frequencies ($f = 40$ GHz, 60 GHz and 80 GHz). Here, $B_m = 900$ mT. (b) The velocities versus time for diffrernt excitation frequency, with $B_m = 900$ mT. (c) The velocity versus time for different excitation amplitude at $f = 100$ GHz.

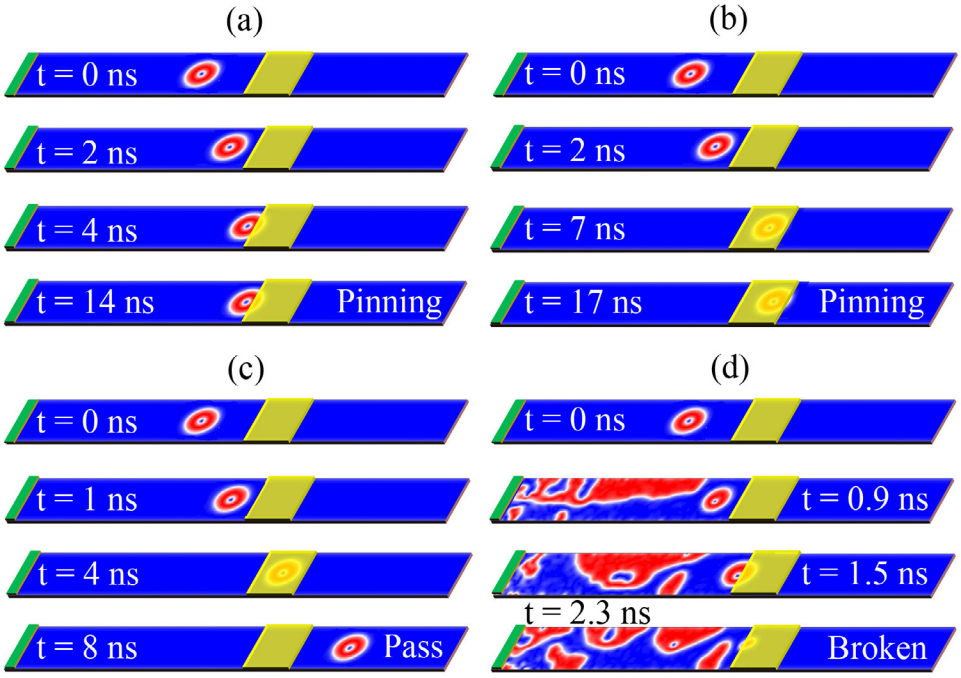

Figure 4. The pinning/depinning states of a 2π-skyrmion driven by spin waves at the first AFM/FM crossing point.

exchange, demagnetizing, DMI, anisotropy and exchange bias of the system as a function of the 2π-skyrmion positions are calculated, as shown in figures 2(b)–(f). In the condition of $H_E > 0$ mT, energy wells are generated in the exchanges and anisotropy energies, contrary to the behavior of the demagnetizing, DMI and exchange bias energies which contribute to the energy barriers in the total energy at the AFM/FM crossing area. In the case of $H_E < 0$ mT, the exchange and anisotropy energies show energy barriers, contrary to the behavior of the demagnetizing, DMI and exchange bias energies which lead to the energy wells in the total energy at the AFM/FM crossing area.

In the following simulations, the dynamics of the pinning process of the 2π-skyrmion is investigated. Spin waves were employed to induce 2π-skyrmion motion. Initially, we investigated the 2π-skyrmion motion driven by spin waves. Figure 3(a) shows the representative 2π-skyrmion position in the x-direction as a function of time, with $B_m = 900$ mT. The insets exhibits the top-views of the 2π-skyrmion motion in a racetrack at selected conditions ($f = 40$ GHz, 60 GHz and 80 GHz; $B_m = 900$ mT). It can be seen that there are some specific frequencies to drive 2π-skyrmions motion effectively, such as $f = 100$ GHz, $B_m = 900$ mT. In some specific frequencies ($f = 40$ GHz, 60 GHz and 80 GHz; $B_m = 900$ mT), spin waves lead to the generation of magnetic domains, which will significantly change the properties of the spin waves guide. These discrete frequencies for the 2π-skyrmion motion may be ascribed to the internal oscillation modes of a 2π-skyrmion and can be related to the variation of the amplitude of the spin waves [13, 15, 29]. With $f = 100$ GHz, $B_m = 900$ mT, the 2π-skyrmions accelerates and then decelerates and can reach a maximum velocity of 95 m s^{-1}(figure 3(b)). Furthermore, in the condition of $f = 100$ GHz, the 2π-skyrmion mobility increases with the excitation amplitude increasing (figure 3(c)).

Then, we investigated the dynamics of the pinning process of the 2π-skyrmion at the first AFM/FM crossing area. As shown in figure 4, when spin waves propagate along the $+x$-direction, there are three cases at the first AFM/FM crossing area: (a) Pinning state: if the driving force is not enough,

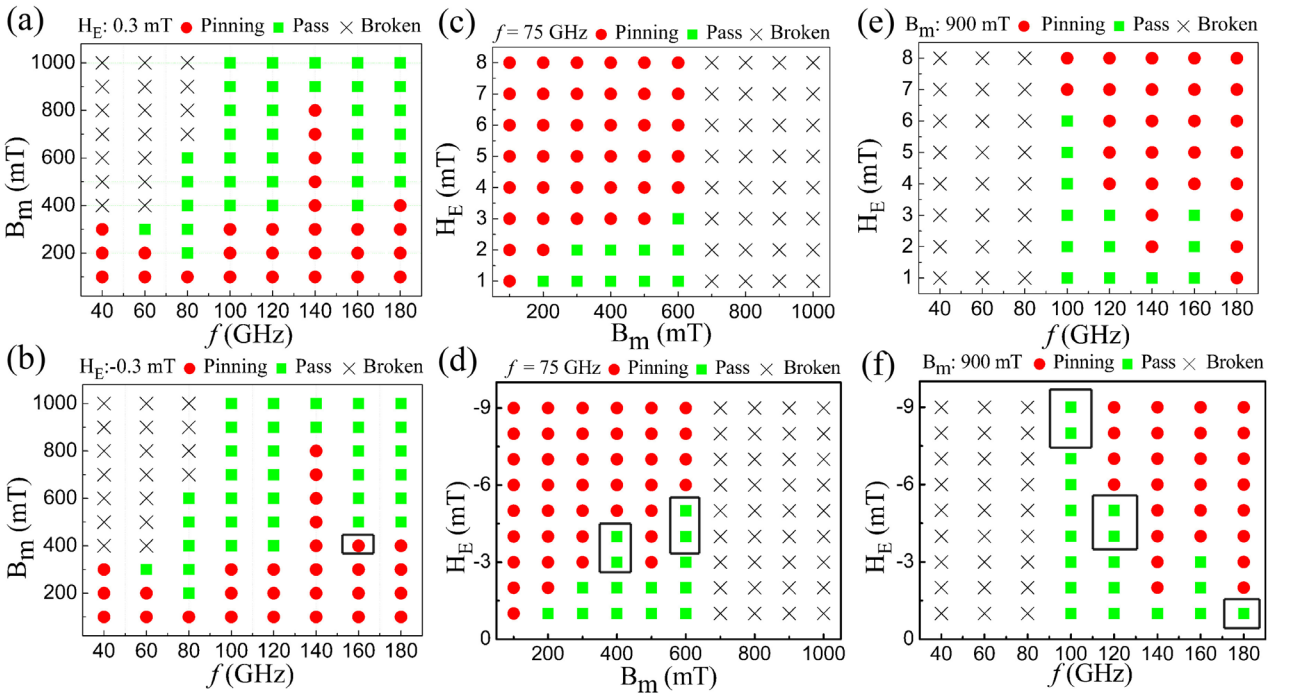

Figure 5. The working window for a 2π-skyrmion in a racetrack as a function of the excitation field amplitude B_m, the excitation frequency f and the exchange bias field.

e.g. $f = 80$ GHz, $B_m = 100$ mT and $H_E = \pm 0.3$ mT, the 2π-skyrmion stops at the left or right boundary of the AFM/FM crossing area; (b) Pass state: if the driving force is enough, the 2π-skyrmion can successfully pass the AFM/FM crossing area, for example, $f = 80$ GHz, $B_m = 400$ mT and $H_E = 0.3$ mT; (c) Broken state: if the driving force is too larger, like $f = 80$ GHz, $B_m = 900$ mT and $H_E = 0.3$ mT, the 2π-skyrmion is broken up owing to the multidomain states. Hence, the AFM/FM crossing area can serve as the pinning sites for the 2π-skyrmion. It was worth noting that the 2π skyrmion is off-centered pinned in the case of $H_E > 0$ mT, whereas it is pinned in a well centered position in the condition of $H_E < 0$ mT. The pinning positions are in agreement with the energy profile in figure 2.

The influence of the exchange bias on the 2π-skyrmion pinning/depinning states at the first AFM/FM crossing area are also investigated. Figures 5(a) and (b) shows the working window for a 2π-skyrmion as a function of the excitation field amplitude B_m and the excitation frequency f, with $H_E = \pm 0.3$ mT. In the condition of $H_E = 0.3$ mT and $B_m = 400$ mT, the 2π-skyrmion is pinned at 140 GHz and 180 GHz, and pass through the racetrack at 80 GHz, 100 GHz, 120 GHz and 160 GHz. With $f = 40$ GHz and 60 GHz, the 2π-skyrmion is broken up at $B_m > 400$ mT. These discrete frequencies for the pinning/depinning of a 2π-skyrmion may be ascribed to the internal oscillation modes of a 2π-skyrmion and can be related to the variation of the amplitude of the spin waves [13, 15, 29]. In the case of $H_E = -0.3$ mT, as shown in figure 5(b), the pinning/depinning states of the 2π-skyrmion is almost the same as that of $H_E = 0.3$ mT, except for the case of $f = 160$ GHz and $B_m = 400$ mT.

Figures 5(c)–(f) show the working windows of a 2π-skyrmion as a function of the exchange bias field at the first

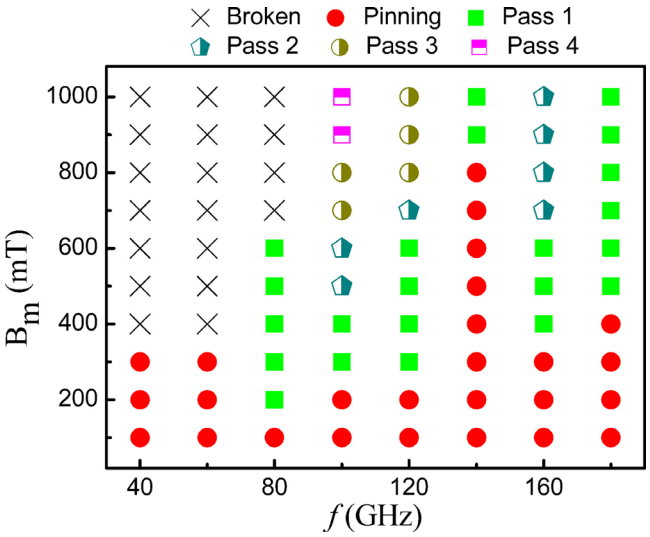

Figure 6. The working window for a 2π-skyrmion in a racetrack with four AFM wires. Here, the exchange bias field is -0.3 mT. Pass 1, Pass 2, Pass 3 and Pass 4 means the 2π-skyrmion can pass the first, the second, the third and the fourth AFM/FM crossing area, respectively.

AFM/FM crossing area. Under the condition of $H_E > 4$ mT and $B_m < 600$ mT, the 2π-skyrmion will be always pinned at $f = 75$ GHz. Given a special excitation field amplitude of $B_m = 900$ mT, the pinning/depinning states exhibit the dependence of the excitation frequency. For example, the 2π-skyrmion can pass through the racetrack even $H_E = 6$ mT at $f = 100$ GHz, while it becomes pinned even $H_E = 1$ mT at $f = 180$ GHz. When f ranges from 100 GHz to 180 GHz and H_E is larger than 7 mT, the 2π-skyrmion is pinned. In the case of $H_E < 0$ mT, the pinning/depinning states is almost the same as that of $H_E < 0$ mT,

except for several cases demonstrated in figures 5(d) and (f). Hence, the exchange bias field, the excitation amplitude and the excitation frequency have a marked impact on the pinning/depinning behavior of a 2π-skyrmion in a racetrack.

Next, a series of transversal AFM wires are set above the FM racetrack. Figure 6 shows the pinning/depinning behaviors of the 2π-skyrmion in a racetrack with four AFM wires. Here, $H_{\mathrm{E}} = -0.3$ mT. With $f = 80$ GHz, $B_{\mathrm{m}} = 100$ mT, the 2π-skyrmion stops at the first AFM/FM crossing area. With $f = 80$ GHz, $B_{\mathrm{m}} = 400$ mT, the 2π-skyrmion can pass the first AFM wire and stops at the second AFM/FM crossing area, since the distance between the spin wave source and the 2π-skyrmion can affect the 2π-skyrmion motion [13, 15]. With $f = 100$ GHz and $B_{\mathrm{m}} = 900$ mT, the 2π-skyrmion can pass all the four AFM/FM crossing area.

To qualitatively understand the dynamics of the 2π-skyrmion pinning in the AFM/FM crossing area, an analytical model is derived. Here, we consider the skyrmion as a rigid structure (without any or with very slight structure deformation). The Thiele approach based on the course-grain approximation can be employed to analytically model the 2π-skyrmion dynamics [30]:

$$\mathbf{G} \times \mathbf{v}_{\mathrm{d}} + \mathcal{D}\alpha\mathbf{v}_{\mathrm{d}} = \mathbf{F}_{\mathrm{sw}} + \mathbf{F}_{\mathrm{AFM}} + \mathbf{F}_{\mathrm{edge}}. \tag{3}$$

The vector $\mathbf{G} = 4\pi Q\mathbf{e}_z$, where $Q = (1/4\pi)\int \mathbf{m} \cdot (\partial_x\mathbf{m} \times \partial_y\mathbf{m})\mathrm{d}S$ is the 2π-skyrmion number. The tensor element $\mathcal{D}_{ij}$ is given by $\mathcal{D}_{ij} = \int (\partial_i\mathbf{m} \cdot \partial_j\mathbf{m})\mathrm{d}x\mathrm{d}y$. The force $\mathbf{F}_{\mathrm{edge}}$ origins from the repulsive potential if the system is finite, namely the boundary effects. The force $\mathbf{F}_{\mathrm{sw}}$ origins from the moment transfer between the spin wave current and the 2π-skyrmion. Accroding to the references, the force $\mathbf{F}_{\mathrm{SW}}$ can be expressed as [15]:

$$F_{\mathrm{sw}}(R) = j e^{\frac{\widehat{r\cdot q}}{L_{\mathrm{SW}}}} |q|^2 \sigma_{\parallel} \widehat{x}. \tag{4}$$

Here, j is the spin-wave current density; the wave vetor $\mathbf{q} = q\widehat{x}$; $\sigma_{\parallel}$ is related to the skew scattering angle of the spin wave; $1/L_{\mathrm{sw}} \approx \alpha\sqrt{2\pi mf/2\hbar}$, where m and f are the spin wave mass and frequency. The exponential term is the approximation form, indicating the decay of the spin-wave current on the scale relating to the Gilbert damping. The equation (4) qualitatively agrees with the simulations of the 2π-skyrmion motion driven by spin waves, namely, the longitudinal component of the velocity is attributed to the longitudinal scattering section of the 2π-skyrmion [15].

The force $\mathbf{F}_{\mathrm{AFM}}$ origins from the exchange bias field from the AFM wires, which can be expressed as:

$$F_{\mathrm{AFM}} = -\nabla U_{\mathrm{AFM}} \tag{5}$$

where ∇U_{AFM} is the variation of total energy of the system. Accroding to the equations (3)–(5) and $\mathbf{G} = 0$, the 2π-skyrmion motion is decomposed into the x-component and y-component:

$$\mathcal{D}\alpha v_x = \mathbf{F}_{\mathrm{SW}} + \mathbf{F}_{\mathrm{AFM}} = j e^{\frac{\widehat{r\cdot q}}{L_{\mathrm{SW}}}} |q|^2 \sigma_{\parallel} \widehat{x} - \nabla U_{\mathrm{AFM}} \tag{6}$$

$$v_y = 0. \tag{7}$$

According to the equation (6), the 2π skyrmion pinning/depinning states depends on the competion of the driving force and the variation of total energy induced by the AFM wires. Combined with the energy profile in the figure 2, the anan-lysis model qualitatively agrees with the simulation results of the dynamics of the pinning/depinning process of the 2π skyrmion.

4. Conclusions

In summary, the pinning/depinning behavior of a 2π-skyrmion using exchange bias has been systematically investigated. The results show that the AFM/FM crossing area can serve as pinning sites for 2π-skyrmion motion. The working windows for a 2π-skyrmion in a racetrack as a function of the exchange bias field, the excitation field amplitude and the excitation frequency are systematically studied. The interaction mechanism between the 2π-skyrmion and the exchange bias is also studied. This work may provide guidance for the design of next-generation spintronics.

Acknowledgments

The authors would like to acknowledge the financial support from the National Natural Science Foundation of China (11574121 and 51771086).

ORCID iDs

Jianbo Wang https://orcid.org/0000-0002-4203-8336
Qingfang Liu https://orcid.org/0000-0001-6533-2880

References

[1] Sampaio J, Cros V, Rohart S, Thiaville A and Fert A 2013 *Nat. Nanotechnol.* **8** 839
[2] Romming N, Hanneken C, Menzel M, Bickel J E, Wolter B, Bergmann K, Kubetzka A and Wiesendanger R 2013 *Science* **341** 636
[3] Zhou S, Wang C, Zheng C and Liu Y 2020 *J. Magn. Magn. Mater.* **493** 165740
[4] Leonov A O, Monchesky T L, Romming N, Kubetzka A, Bogdanov A N and Wiesendanger R 2016 *New J. Phys.* **18** 065003
[5] Zhang S, Kronast F, Laan G and Hesjedal T 2018 *Nano Lett.* **18** 1057
[6] Zheng F *et al*2017 *Phys. Rev. Lett.* **119** 197205
[7] Finazzi M, Savoini M, Khorsand A R, Tsukamoto A, Itoh A, Duo L, Kirilyuk A, Rasing T and Ezawa M 2013 *Phys. Rev. Lett.* **110** 177205
[8] Cortés-Ortuño D, Romming N, Beg M, Bergmann K, Kubetzka A, Hovorka O, Fangohr H and Wiesendanger R 2019 *Phys. Rev.* B **99** 214408
[9] Kent N *et al* 2019 *Appl. Phys. Lett.* **115** 112404
[10] Zhang X, Xia J, Zhou Y, Wang D, Liu X, Zhao W and Ezawa M 2016 *Phys.Rev.* B **94** 094420
[11] Kolesnikov A G, Stebliy M E, Samardak A S and Ognev A V 2018 *Sci. Rep.* **8** 16966
[12] Booth A C, Liu Y and Zang J 2019 *J. Magn. Magn. Mater.* **489** 165447

[13] Shen M, Zhang Y, Jun O Y, Yang X and You L 2018 *Appl. Phys. Lett.* **112** 062403
[14] Pylypovskyi O V, Makarov D, Kravchuk V P, Gaididei Y, Saxena A and Sheka D D 2018 *Phys. Rev. Appl.* **10** 064057
[15] Li S, Xia J, Zhang X, Ezawa M, Kang W, Liu X, Zhou Y and Zhao W 2018 *Appl. Phys. Lett.* **112** 142404
[16] Hanneken C, Kubetzka A, Bergmann K and Wiesendanger R 2016 *New J. Phys.* **18** 055009
[17] Bhatti S, Sbiaa R, Hirohata A, Ohno H, Fukami S and Piramanayagam S N 2017 *Mater. Today* **20** 530
[18] Kang W, Huang Y, Zheng C, Lv W, Lei N, Zhang Y, Zhang X, Zhou Y and Zhao W 2016 *Sci. Rep.* **6** 23164
[19] Fook H T, Gan W L and Lew W S 2016 *Sci. Rep.* **6** 21099
[20] Toscano D, Leonel S A, Coura P Z and Sato F 2019 *J. Magn. Magn. Mater.* **480** 171
[21] Reichhardt C and Reichhardt C J O 2019 *Phys.Rev.* B **99** 104418
[22] Polenciuc I, Vick A J, Allwood D A, Hayward T J, Vallejo-Fernandez G, O'Grady K and Hirohata A 2014 *Appl. Phys. Lett.* **105** 162406
[23] Donahue M J and Porter D G 2009 OOMMF User's Guide Version 1.0, Interagency Report NISTIR
[24] Rohart S and Thiaville A 2012 *DMExchange6Ngbr* (http://math.nist.gov/oommf/contrib/oxsext/)
[25] Dijken S, Moritz J and Coey J M D 2005 *J. Appl. Phys.* **97** 063907
[26] Meiklejohn W H and Bean C P 1956 *Phys. Rev.* **102** 1413
[27] Meiklejohn W H 1962 *J. Appl. Phys.* **33** 1328
[28] Rózsa L, Hagemeister J, Vedmedenko E Y and Wiesendanger R 2018 *Phys. Rev.* B **98** 224426
[29] Seo S M, Lee H W, Kohno H and Lee K 2011 J, *Appl. Phys. Lett.* **98** 012514
[30] Thiele A 1973 *Phys. Rev. Lett.* **30** 230